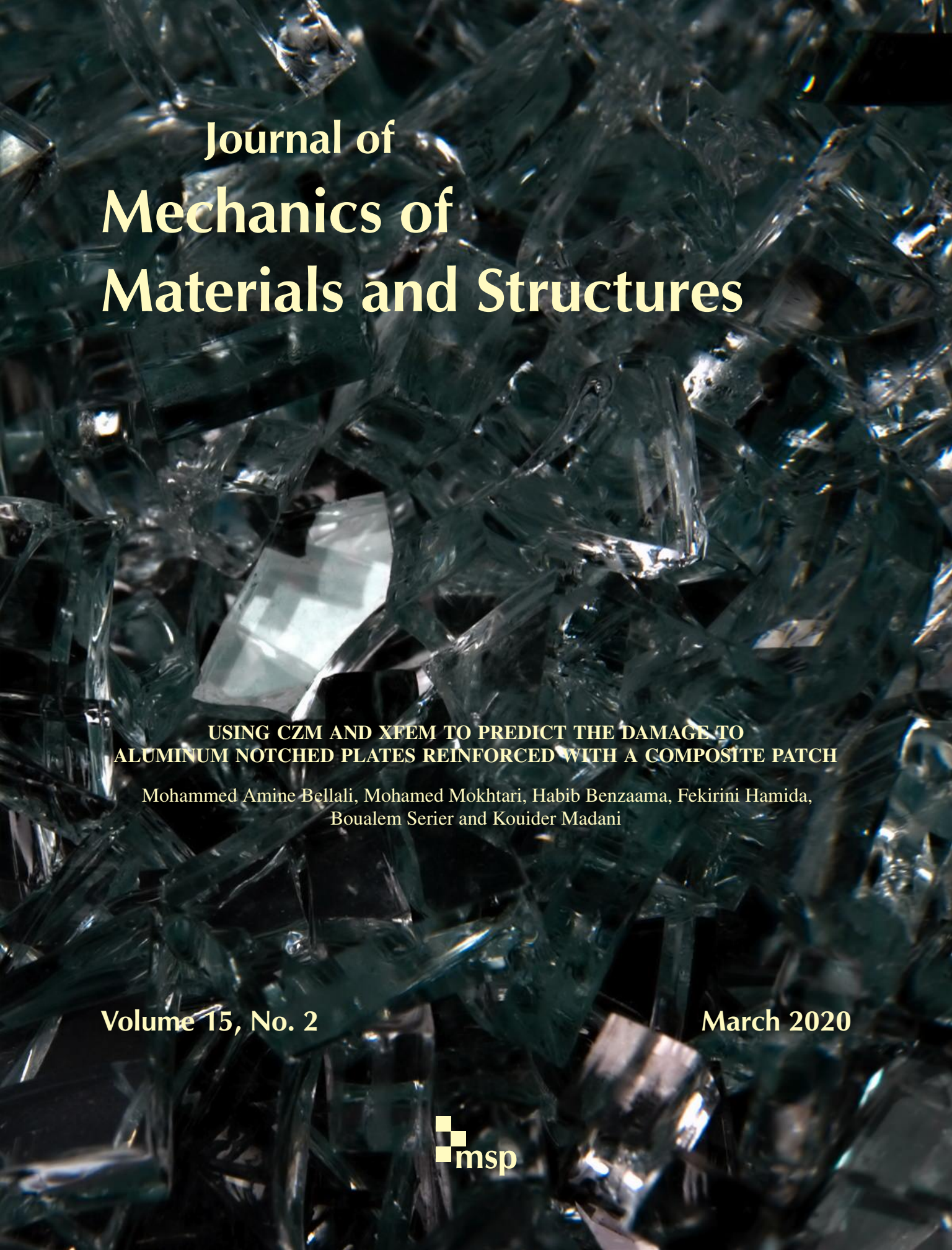

Journal of
Mechanics of
Materials and Structures

USING CZM AND XFEM TO PREDICT THE DAMAGE TO ALUMINUM NOTCHED PLATES REINFORCED WITH A COMPOSITE PATCH

Mohammed Amine Bellali, Mohamed Mokhtari, Habib Benzaama, Fekirini Hamida, Boualem Serier and Kouider Madani

Volume 15, No. 2 March 2020

msp

JOURNAL OF MECHANICS OF MATERIALS AND STRUCTURES
Vol. 15, No. 2, 2020
dx.doi.org/10.2140/jomms.2020.15.185

USING CZM AND XFEM TO PREDICT THE DAMAGE TO ALUMINUM NOTCHED PLATES REINFORCED WITH A COMPOSITE PATCH

MOHAMMED AMINE BELLALI, MOHAMED MOKHTARI, HABIB BENZAAMA, FEKIRINI HAMIDA, BOUALEM SERIER AND KOUIDER MADANI

The competition between the propagation of cracks in the plate and the detachment of the patch has been invested in this work. Our goal is to analyze the damage of a notched plate reinforced by a composite patch using FEM. The effect of several parameters of the plate/cohesive/patch structure was evaluated. These parameters concern: firstly, the composite patch such as its stacking sequence; secondly, for the plate we consider the size and shape of the notch; finally, the cohesive area that is conditioned by its resistance to the mechanism of damage. The effect and competition of these different parameters are evaluated and presented by both load-displacement curves and curves that show the competition between the detachment of the patch and the propagation of the crack in the plate. The calculations are performed with the ABAQUS numerical code using CZM cohesive elements for patch detachment and the XFEM technique for plate fracture. The results obtained illustrate the variation of the damage as a function of these parameters acting simultaneously: the resistance of the interface and the patch under the effect of the notch. Hence these levels of resistance condition the mechanism of damage between the propagation of the crack in the plate and the detachment of the patch.

1. Introduction

In recent years polymeric matrix composite structures have been widely used in a number of sectors, particularly for the advantageous weight/resistance ratio [Elhannani et al. 2016]. They can also be used for repairing patch structures. On the other hand, the notched structures are widely presented in the concepts from where the need for their reinforcement often by composite patches. These structures are still subject to damage and their modes of rupture sometimes result in defects. Among them, the patch/plate detachment mode is the most common and often occurs by a low adhesive strength between patch/plate layers for many reasons.

Using the finite element method (FEM) by ABAQUS software, Ait Kaci et al. [2017] has investigated the effects of composite patch repair of a cracked aluminum plate. This gives the advantage of meshing the structure automatically after each step of the growth of the crack. Other researchers such as Mohamed and Bouiadjra [2016] optimized the shape of the repair patch on a cracked plate.

A new technique known as Xtended finite element method (XFEM) has been implemented for numerical modeling of crack propagation. This numerical approach was presented in [Benzaama et al. 2018]. A modified function is implemented to model the surface of the crack by adding additional degrees of freedom to each node so-called “enriched elements”.

Mokhtari is the corresponding author.
Keywords: repair technique, CZM (cohesive zone model), XFEM (Xtended finite element method), adhesive type.

Further improvements to XFEM have been presented in different applications with plastic/elastic domains, fluid/solid phases, and static/dynamic loads. Most researchers have focused on interlaminar cracking as in composite materials. The energy criteria are based on the mechanics of fracture, used to predict the onset and growth of detachment. Among them, the virtual crack closure technique (VCCT) and the cohesive zone method (CZM) are the two prediction methods based on the comparison of energy between the strain energy release rate (G) and the energy release rate (GC). VCCT requires an initial crack in the mesh prior to crack propagation analysis. Other work by Ezzine et al. [2018] includes an experimental and numerical study using CZM and XFEM methods. Many studies are working on the breaking behavior of the interface layers such as [Song et al. 2016] and [Ibrahim et al. 2016], the CZM use as well by [Jiao et al. 2017] in the debonding between FRP and concrete the CZM show some disadvantages such as the introduction of softening and instability of the numerical computation, in particular during the propagation of cracks. But it remains the method most used by researchers since it does not require an initial crack and has greater advantages for cracking in mixed mode.

In most studies of cracked and composite repaired structures, the phenomenon of debonding is no longer considered as crack propagation when they should be modeled. The ABAQUS software is used to better simulate the results of a structure reinforced by a composite patch. The damage analysis referred to in this work is the introduction of the two damage criteria on the same structure. The use of close break parameters clearly shows the creation of a complex damage mechanism. This makes it possible to improve the adequacy between the elements (plate/interface/patch) constituting the structure. In this article, we study these possibilities by evaluating the interaction between the crack propagated in the plate and the detachment of the interfaces between materials having different elastic and breaking properties.

1.1. ***XFEM technique and input parameters.*** The XFEM method consists in a mesh of finite elements which is independent of the discontinuity. This formulation takes off the need to define a new mesh configuration (remeshing) for the simulation of crack propagation, by opposition to the classical FEM. Therefore, the same mesh is used for all time steps during crack propagation. The XFEM is based on the introduction of additional degrees of freedom which are established in the nodes of the elements that are intersected by the crack geometry.

The XFEM uses the concept of partition of finite element unity and enrichment function. The enrichment functions are expressed as [Moës et al. 1999]

$$U_{\mathrm{XFEM}}(X) = \sum_{i\in\Gamma} Ni(X)\,ui + \sum_{i\in J} Ni(X)\,H(X)\,ai + \sum_{i\in K} Ni(X)\left[\sum_{\alpha=1}^{4} F\alpha(X)\,bi\alpha\right], \tag{1}$$

where Γ is the set of all nodes in the mesh, $Ni(X)$ is the nodal shape function and ui is the standard degree of freedom (DOF) of node i (ui represents the physical nodal displacement for nonenriched nodes only). The subsets J and K contain the nodes enriched with Heaviside function $H(X)$ or crack-tip function $F\alpha(X)$, respectively, and $(ai, bi\alpha)$ are the corresponding DOFs.

In (1) the first and second term on the righthand side is applicable to all nodes in the model; the third term is valid for nodes whose shape function support is cut by the crack interior and the third term is used only for nodes whose shape function support is cut by the crack tip [Qian and Jing 2012]. The

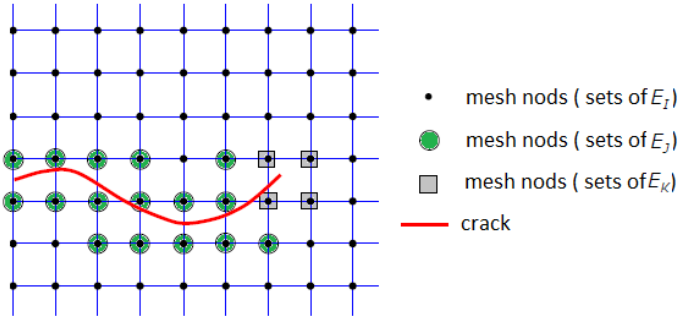

Figure 1. Description of the E_1, E_J and E_K sets of the displacement field approximation enriched finite element.

Heaviside function $H(X)$ is defined as

$$H(x) = \begin{cases} -1 & \text{if } x > 0, \\ 1 & \text{if } x < 0. \end{cases} \tag{2}$$

The crack-tip function $F\alpha(X)$ contains the enrichment functions (branch functions) used to increase the accuracy of the numerical solution around crack tip and their formulation depends on the nature of the problem to be solved. For LEFM problems, these functions are chosen based on the asymptotic behavior of the displacement field at the crack tip [Belytschko and Black 1999]:

$$F\alpha(X) = \left[\sqrt{r}\sin\frac{\theta}{2}, \sqrt{r}\cos\frac{\theta}{2}, \sqrt{r}\sin\theta\sin\frac{\theta}{2}, \sqrt{r}\sin\theta\cos\frac{\theta}{2}\right], \tag{3}$$

where (θ, r) denotes a polar coordinate system with its origin at the crack tip and when $\theta = 0$ it is tangent to the crack at the tip; $\sqrt{r}\sin(\theta/2)$ takes into account the discontinuity across the crack face. This function has a lot of applications including biomaterial and elastic-plastic power law hardening material. The structure domain is created as a solid, the XFEM enrichment domain function with the crack is the hole and input order as

```
*Enrichment,  name = Crack-1,  type = PROPAGATION CRACK,  activate = ON.
```

The evaluated damage is maximal at crack opening and is calculated using

$$\delta_n = \sqrt{\left(\langle\delta_n\rangle^2 + \delta_s^2 + \delta_t^2\right)}. \tag{4}$$

The following analysis uses the elastic properties presented in Table 1. The maximum principal stress is the value of the unnotched nominal strength measured as 456 MPa. The damage evaluation criterion is the maximum traction displacement (maximum crack opening of aluminum measured as 0.14 mm).

yield stress $(R_{0.2}) = 310$ MPa	maximum stress $(R_{\mathrm{m}}) = 452$ MPa
percentage elongation $(A) = 2.4\%$	$E = 68.8$ GPa, $\nu = 0.33$

Table 1. Material mechanical properties of aluminum 2024-T3.

1.2. ***Cohesive interfaces and input parameters.*** The damage evolution model is a linear tensile-separation law as shown in Figure 2, defined by a surface of nodes in a mesh where no interaction has been introduced between the surfaces. The cohesive law contains an undamaged initial regime of elastic behavior where the surfaces are attached to each other. The damage path is entirely in the cohesive zone.

A damage initiation stress threshold is defined; it initiates a softening regime behavior where the stiffness degradation increases as the surfaces move away from each other. Finally, both surfaces reach a separation level so that the stiffness connecting them is zero and they are completely "detached" from each other. For damage initiation, a quadratic traction criterion was used for a mixed mode defined in (5).

The cohesive interfaces were modeled using the traction-separation implementation in ABAQUS (see Figure 3). The input of the stiffness parameters (K_{nn}, K_{ss} and K_{tt}) required by ABAQUS is the modulus of the cohesive material divided by its thickness. The model requires knowledge of local forces ($\sigma_{u,i}$, $i = \mathrm{I}, \mathrm{II}, \mathrm{III}$) and critical stress energy release rates (G_i, $i = \mathrm{I}, \mathrm{II}, \mathrm{III}$).

When (2) is satisfied, the constraints are completely released. The evolution of cohesive damage is based on energy defined by the Benzeggagh–Kenane criterion. The zones of the triangle correspond to the critical breaking energy introduced such that $G_{\mathrm{I}} = 0.3\,\mathrm{N/m}$ (normal structure, Mode I) and $G_{\mathrm{II}} = G_{\mathrm{III}} = 0.6\,\mathrm{N/m}$ (shear structure, Mode II and Mode III) are used [Campilho et al. 2013; Mokhtari et al. 2017]. The debonding (opening and spreading) can only take place by the failure of these elements under

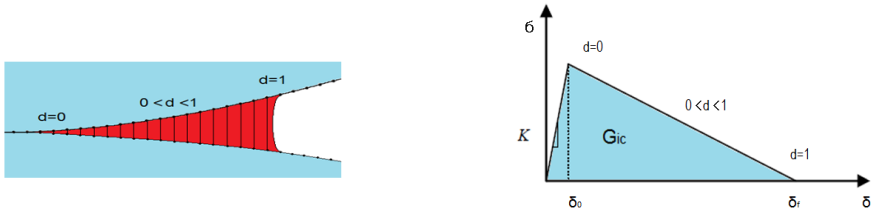

Figure 2. Linear softening law for mixed-mode cohesive damage models.

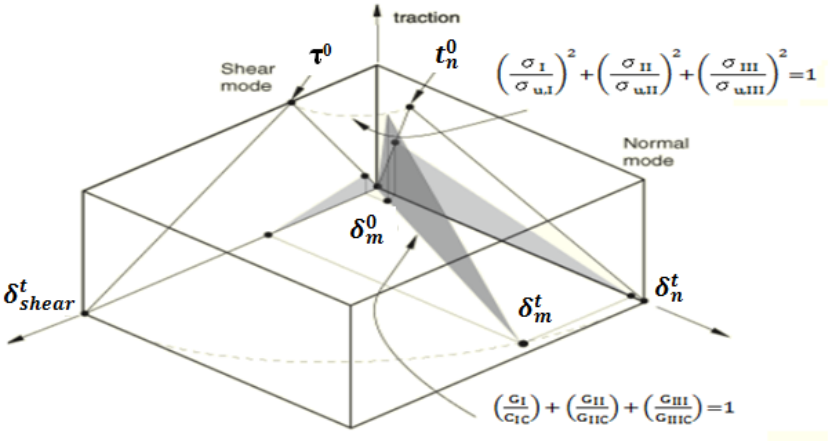

Figure 3. A traction-separation law for modeling the interface material degradation.

load condition and failure criteria. The quadratic stress criterion can be written as

$$\left(\frac{\sigma_{\mathrm{I}}}{\sigma_{u,\mathrm{I}}}\right)^2+\left(\frac{\sigma_{\mathrm{II}}}{\sigma_{u,\mathrm{II}}}\right)^2+\left(\frac{\sigma_{\mathrm{III}}}{\sigma_{u,\mathrm{III}}}\right)^2=\begin{cases}1, & \text{if } \sigma_1\geq 0,\\ 0, & \text{if } \sigma_1\leq 0.\end{cases} \tag{5}$$

where σ_i $(i=\mathrm{I},\mathrm{II},\mathrm{III})$ represent the stresses at a given integration point of the interface finite element in each mode. Mode I is the local opening mode and modes II, III the shear modes at the interface. The crack propagation was simulated by the linear energetic criterion

$$\left(\frac{G_{\mathrm{I}}}{G_{\mathrm{IC}}}\right)+\left(\frac{G_{\mathrm{II}}}{G_{\mathrm{IIC}}}\right)+\left(\frac{G_{\mathrm{III}}}{G_{\mathrm{IIIC}}}\right)=1. \tag{6}$$

1.3. ***Finite element modeling.*** A series of sensitivity analyzes was performed to evaluate the effect of modeling parameters on the variation of numerical predictions. For reliable simulations, the geometry of the numerical model has been realized in one part. Each criterion of damage is attached to its region. The patch/plate interface is composed of cohesive elements in order to model the detachment. The XFEM criterion is used for the plate to model crack initiation and propagation. In the sense of numerical computation, the studied parameters are in close agreement with the computational convergence. On the other hand, if the cohesive zone would introduce global softening to the simulation, it can lead to underestimation of the maximum peel release force. To cope with this problem, a viscosity coefficient of $10\cdot 10^5$ was chosen with an adequate time increment for the stabilization of the cohesive damage calculation. A fine mesh with identical elements was recommended according to the thickness (plate/patch) and around the cohesion zone, in order to analyze the separation in mixed mode between the composite and the plate. The use of the XFEM technique in the damage of the aluminum plate makes it possible to have more precise and stable solutions than the results obtained by conventional finite elements. The latter were rough or very oscillatory. Another advantage of the XFEM is that the finite element mesh in this technique is generated independently of the location of the discontinuities.

2. Description of model geometry and material properties

Consider a thin 2024-T3 elastic aluminum plate having height $H=150\,\mathrm{mm}$, width $W=50\,\mathrm{mm}$, thickness $e=2\,\mathrm{mm}$. Notches of different shapes and sizes are taken for each plate. These plates are subjected to an imposed displacement of 4 mm. The composite patch is bonded to the plate to strengthen and reduce the tension of the damaged area through the adhesive. The dimensions of the patch composite are: length $H_r=50\,\mathrm{mm}$, width $W_r=50\,\mathrm{mm}$ and thickness $e_r=2\,\mathrm{mm}$. The geometric model of finite elements is represented in Figure 4.

Tensile tests performed on 2024-T3 aluminum plate have allowed us to have the characteristic curves shown in Figure 5 (left) [Madani et al. 2010]. From this curve, we can determine the mechanical properties of the material (see Table 1).

The stress-strain relationship in the nonlinear part of the plasticity of aluminum as well as the coordinates of the last point of the breakpoint curve were introduced in the ABAQUS code as damage parameters to simulate an increased failure/damage level after the ultimate stress was reached. So the model of plasticity extends beyond the ultimate stress.

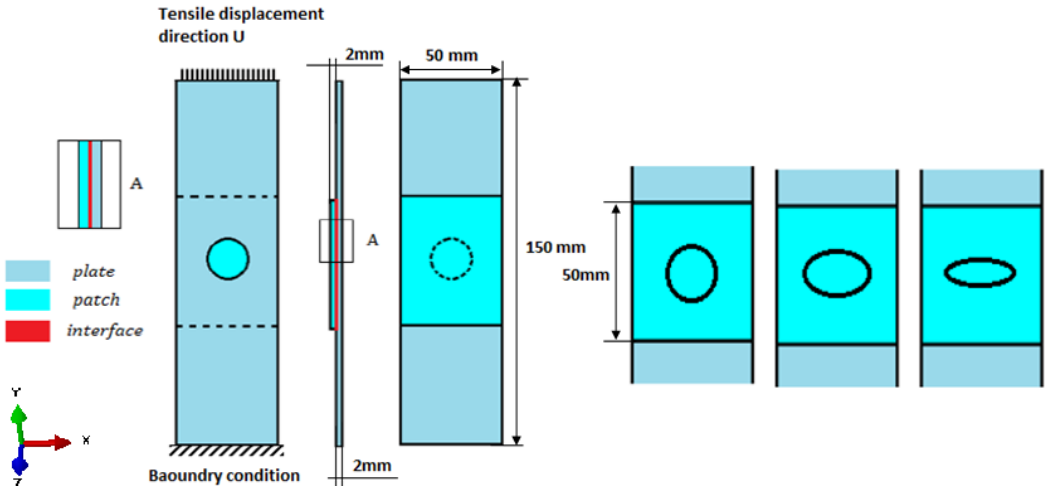

Figure 4. Geometric model of the bonded system.

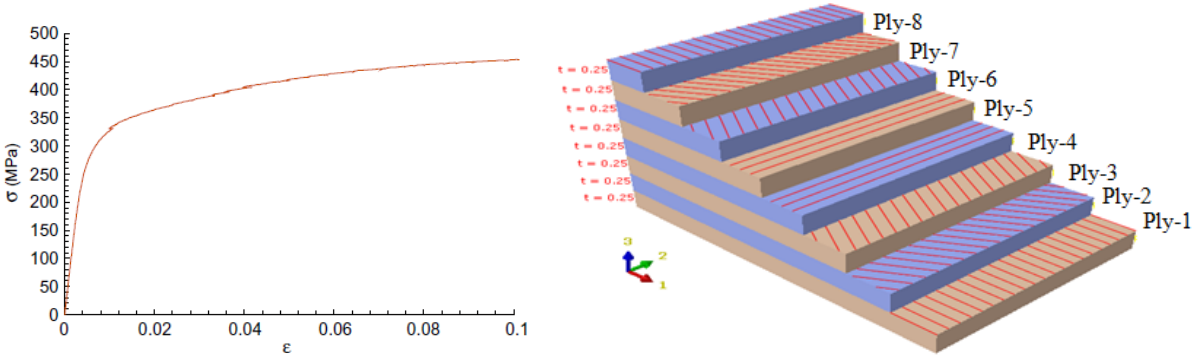

Figure 5. Left: tensile stress-strain curve of aluminum plate. Right: the stacking sequence of composite used.

The interlaminar rupture of the composite patch was not considered in this analysis. This is to promote only the separation between the plates (composite/aluminum). The geometry of the composite is presented in Figure 5 (right). The analysis was carried out for a composite laminates namely, carbon epoxy. The properties of the composite used in this study are listed in Table 2.

Young's modulus, E	Poisson's ratio, ν	shear modulus, G
$E_1 = 109000$ MPa	$\nu_{12} = 0.342$	$G_{12} = 4315$ MPa
$E_2 = 8819$ MPa	$\nu_{13} = 0.342$	$G_{13} = 4315$ MPa
$E_3 = 8819$ MPa	$\nu_{23} = 0.380$	$G_{23} = 3200$ MPa

Table 2. Mechanical properties of the laminates used [Mokhtari et al. 2017].

laminate 1: $(0_8)_S$	laminate 4: $(0_2/45_2/-45_2/90_2)_S$
laminate 2: $(0_2/15_2/-15_2/90_2)_S$	laminate 5: $(0_2/60_2/-60_2/90_2)_S$
laminate 3: $(0_2/30_2/-30_2/90_2)_S$	laminate 6: $(0_2/75_2/-75_2/90_2)_S$

Table 3. Different ply orientations used in analyses [Mokhtari et al. 2017].

Different ply orientations of the composite patch are considered in this study to investigate their effect on the failure load. The value of orientation angle (θ) is taken from the longitudinal direction of the structure (x-axis) and varied from 0° to 90° (Table 3). All layers have the same matrix (epoxy) and the same fiber materials (carbon). The numbers 1, 2, ..., 6 in Table 3 indicate the laminate types chosen in the x-axis for different curves.

The adhesive used for bonding along this study is Araldite 420 which is used in aerospace industry because of its important mechanical characteristics. Other qualities of adhesive have been used to see their effects on the mechanism of damage. The different mechanical properties of the adhesives are given in Table 4 and are taken directly from the literature. The mechanical properties of the various adhesives as well as their fracture parameters (Table 4) are essential for modeling the cohesive zone.

No assembly has been done; the geometric model has been partitioned by an interface or the three parts plate/cohesive/patch share the same nodes, so the same mesh architecture has been retained for each model. The cohesive element was selected as an interface between the plate and the patch geometrically with zero thickness, its thickness values are introduced into the rigidity of the interface (Figure 6).

To simulate patch detachment with crack propagation in the plate, the linear behavior of the composite and nonlinear aluminum was presented using 13428 elements of C3D8R solid elements for aluminum where XFEM model is implemented and 5554 for the patch. For each structure the number varies with the shape of the notch. Figure 7 shows a detail of the mesh used for the three elements plate/cohesive/patch.

Araldite 420		
$K_{nn} = 9.25 \cdot 10^5\ \mathrm{GN/m^3}$	$K_{ss} = 11.85 \cdot 10^5\ \mathrm{GN/m^3}$	$K_{tt} = 11.85 \cdot 10^5\ \mathrm{GN/m^3}$
$\varrho_{uI} = 40\ \mathrm{MPa}$	$\tau_{uII} = 24.1\ \mathrm{MPa}$	$\tau_{uIII} = 24.1\ \mathrm{MPa}$
$G_{IC} = 0.3\ \mathrm{N/mm}$	$G_{IIC} = 0.6\ \mathrm{N/mm}$	$G_{IIIC} = 0.6\ \mathrm{N/mm}$
cohesive AV138		
$K_{nn} = 2.45 \cdot 10^5\ \mathrm{GN/m^3}$	$K_{ss} = 7.8 \cdot 10^5\ \mathrm{GN/m^3}$	$K_{tt} = 7.8 \cdot 10^5\ \mathrm{GN/m^3}$
$\varrho_{uI} = 39.45\ \mathrm{MPa}$	$\tau_{uII} = 30.2\ \mathrm{MPa}$	$\tau_{uIII} = 30.2\ \mathrm{MPa}$
$G_{IC} = 0.2\ \mathrm{N/mm}$	$G_{IIC} = 0.38\ \mathrm{N/mm}$	$G_{IIIC} = 0.38\ \mathrm{N/mm}$
cohesive 7752		
$K_{nn} = 9.25 \cdot 10^5\ \mathrm{GN/m^3}$	$K_{ss} = 9.5 \cdot 10^5\ \mathrm{GN/m^3}$	$K_{tt} = 9.5 \cdot 10^5\ \mathrm{GN/m^3}$
$\varrho_{uI} = 11.48\ \mathrm{MPa}$	$\tau_{uII} = 10.17\ \mathrm{MPa}$	$\tau_{uIII} = 10.17\ \mathrm{MPa}$
$G_{IC} = 2.36\ \mathrm{N/mm}$	$G_{IIC} = 5.41\ \mathrm{N/mm}$	$G_{IIIC} = 5.41\ \mathrm{N/mm}$

Table 4. Elastic, strength and fracture properties of different adhesives [Campilho et al. 2013].

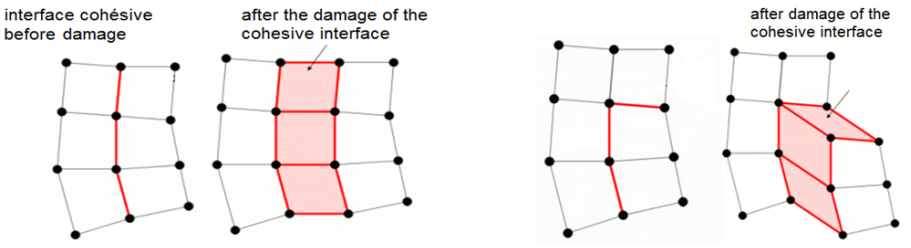

Figure 6. Separation presentation of a cohesive interface.

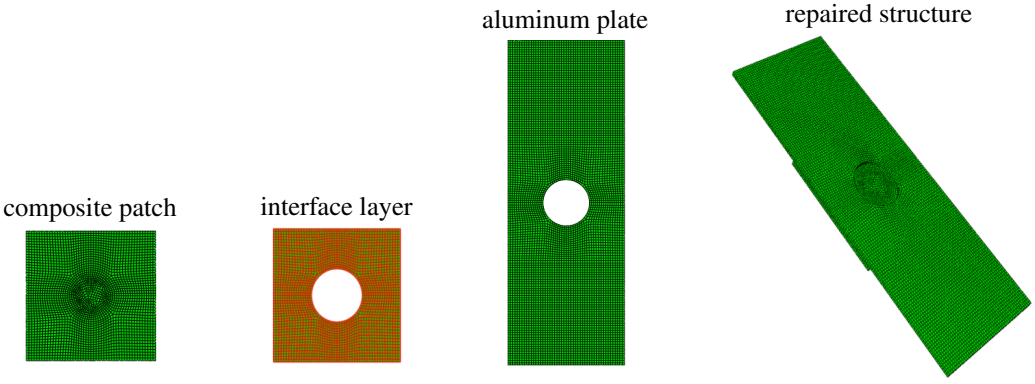

Figure 7. Details of the mesh of each region.

No interaction was introduced between the surfaces. The adhesive was modeled as an interface (zero thickness) with typical elements COH3D8 and a number that exceeds 2214 elements according to the shape of the notch. It is thus necessary to introduce the break parameters (see Table 4).

The debonding was simulated in the finite element model by maintaining the same nodes on both adjacent faces of the overlap area (aluminum/composite). It is necessary to have an appropriate number of mesh elements in the overlapping region on which the damage properties are based. In other words, when the number of nodes increases or decreases there will be no convergence or damage (detachment).

3. Analysis and results

Generally, in repaired structures, the distribution of stresses in the adhesive joint is heterogeneous. Highest stress values are noted along the free edge in contact with the patch and around the damaged area, that is, the notch present in the plate. The rest of the adhesive layer is practically inactive, with low stress values. During the detachment, the adherents (patch/adhesive/plate) play a determining role in the resistance values and the mechanism of the system to the damage. These values are the variables to be evaluated in this study.

3.1. ***Effect of geometrical and dimensional notch of the plate on the damage behavior.*** The presence of a notch in the reinforced plate makes it possible to locate the initiation of the crack and to observe at the same time the effectiveness of the reinforcement patch. The propagation path is a difficult one because it depends on various factors such as the elastic mismatch of the constituent materials and the properties of the interfaces. The objective of this part of the study is to evaluate the effect of the dimensions of

the notch (circular, when $a = b = r$, or elliptic, when $a \neq b$ and one of these parameters at a time is held constant while the other is varied) on the resistance of the repaired plate by the determination of the load-displacement curves.

The evolution of the system to the expected damage presented by the load-displacement curves is a function of the rigidity and the dimensions of the element that constitute the assembly (patch/adhesive/plate). The different figures are accompanied by the result of the plate without reinforcement to better compare it by that of the repaired case.

Figure 8 shows the response of the structure to the imposed load in the presence of a circular notch. The effect of the dimension of the notch is seen to be directly proportional to the resistance of the structure; if the dimension of the notch is minimal, the resistance of the structure is higher. However, the presence of the patch increases the rigidity of the structure up to a high value of the imposed load, which causes its detachment. The reinforcement capacity before peeling is the same for the different dimensions of the notch. On the other hand, after detachment of the patch, an advantage in the resistance of the structure depends on the notches of large dimensions.

For the effect of the elliptical notch when the dimension a is constant, it is noted in Figure 9 that the notch dimensions do not take an important effect in the strength of the structure with or without reinforcement because the damage is completely favored according to dimension a of the notch and there is no effect of the dimension b. The reinforcement in this form of notch is more advantageous and more resistant than that of the unreinforced plate. The effect of the elliptical notch when b is constant shows that the dimensions take an important effect in the strength of the structure; when dimension a increases, the resistance of the structure is lower because it is the zones which promote damage. On the other hand, the reinforcement takes an important effect in the resistance before and after the debonding.

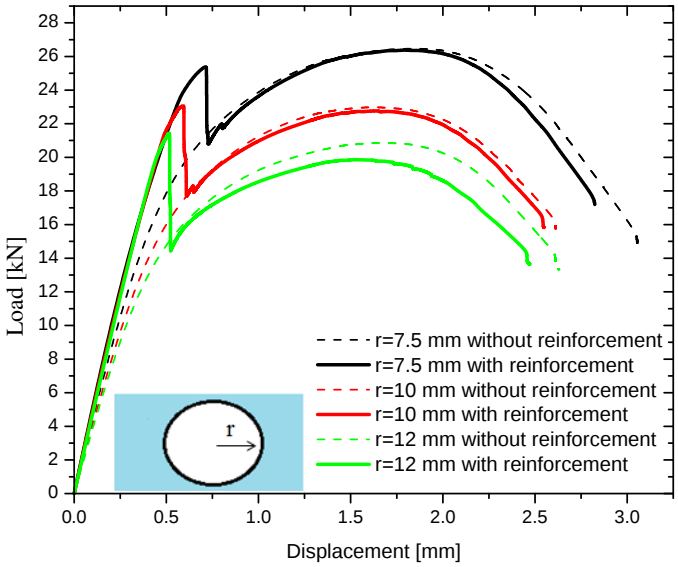

Figure 8. Load-displacement curves for different dimensions (radius) of circular notch (plate repaired with Araldite AV138).

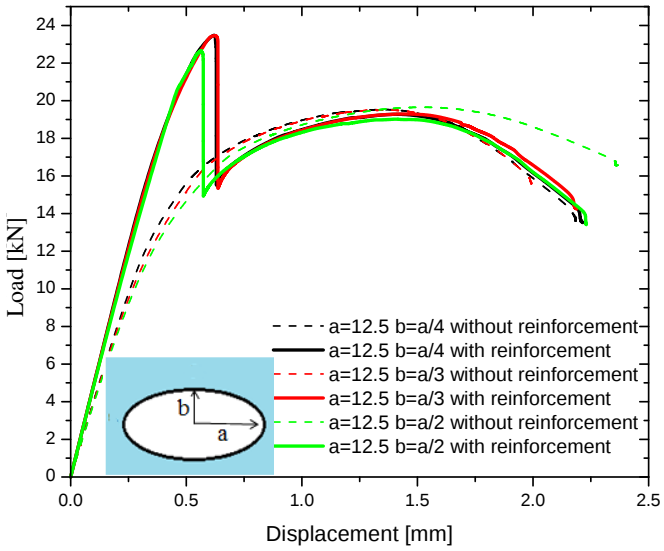

Figure 9. Load-displacement curves for different dimensions of elliptical notch (plate repaired with Araldite AV138).

Figure 10 shows that the effectiveness of the patch in the resistance of the structure is much more conditioned by the shape of the notch only by its size. The advantage of the reinforcement on the strength of the structure is clearly established for the elliptical shape of the notch which has a high stress concentration compared to the circular notch.

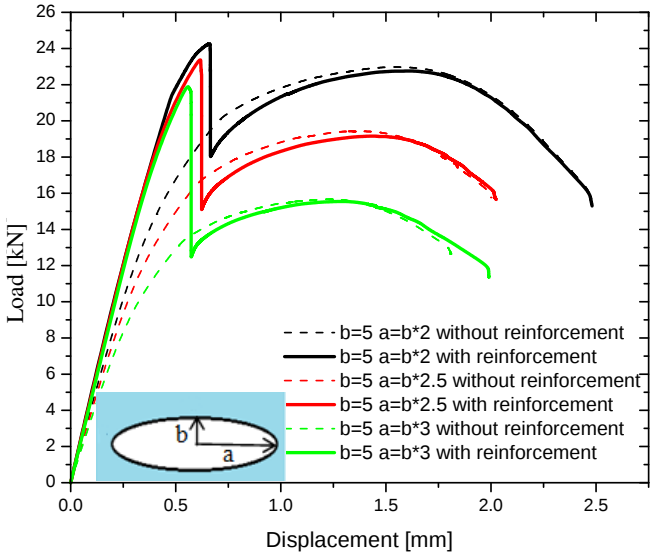

Figure 10. Load-displacement curves for different dimensions of an elliptical notch (plate repaired with Araldite AV138).

If the notch has a significant dimension a, the section of the plate decreases and therefore a low resistance of the plate occurs. However, if the dimension b of the notch increases, its effect is small on the strength of the plate.

3.2. ***Effect of stacking sequence of the patch on the efficiency of reinforcement.*** The objective in this part of the study is to analyze the effect of the stacking sequence on the composite/cohesive/aluminum resistance capacity. Six laminate stacking sequences were selected [Campilho et al. 2013]. In assembled systems, the stiffness of the composite materials that can absorb more load is explained by the orientation of these fibers with respect to the loading axis (stacking sequence effect). This also explains why in some cases separation occurs quickly (B. Varughese 1997). In the case of composite patch reinforcement, the advantage of the stacking sequence will take place only according to the deformability of the plate.

In Figure 11, the stacking sequence effect on the effectiveness of reinforcing the patch on a plate notched with a circular shape at $r = 10$ mm is presented. It uses about 2214 finite elements with a finer mesh in the region where the crack must propagate. The simulation shows identical initial behavior for all stacking sequences until maximum load is reached (Figure 11). Each layer of the composite patch ensures a charge transfer according to the orientation of its fibers and provides the plate with a gain in stiffness until the patch is detached. The system will continue to follow the same path for the different stacking sequences.

It should be noted that as the strength of the adhesive increases, the magnitude of this resistance varies with the variation of the stacking sequence; in other words, with the orientation of the fibers. The combination of fracture energy is quite high and the stacking sequence for which the orientation of the fibers is less than 45°; a value more that 45° gives the system a considerable resistance capability.

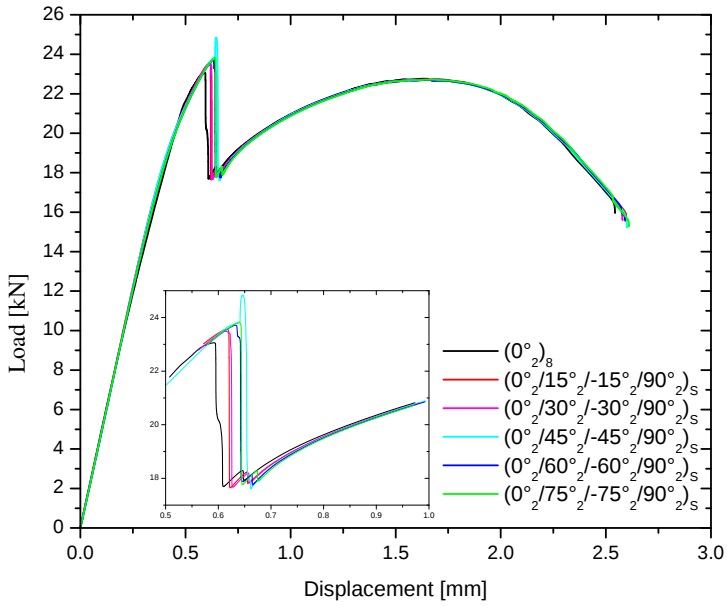

Figure 11. Failure load-displacement curves for different stacking sequences of carbon-epoxy laminate.

3.3. ***Effect of resistant parameter of the adhesive on the efficiency of reinforcement.*** In this part of the study, it is not possible to condition the effect of the fracture parameters of the adhesive. These parameters occur simultaneously by the nature of the adhesive itself. It should be noted of course that the values in mode II are always higher than that in mode I because the adhesives work better in shear than in tension. In most cases, damage to the plate will begin after detachment of the reinforcement patch. The adhesive will continue to withstand efforts to transmit the load until it is able to resist. In addition to other parameters such as S_{nn}, S_{tt}, S_{ss} (normal and tangential strength) and K_{nn}, K_{ss}, K_{tt} (normal and tangential stifness), the separation energy of the G_I, G_{II} and G_{III} adhesive plays the most important role in the strength of the adhesive as shown in the Figure 12. The results show clearly the effectiveness of this type of analysis using the cohesive zone model. It is important to take as reference the unrepaired plate.

When loading the repaired structure by patch, the force-displacement curve goes through stages where few phenomena are observed: propagation of the crack in the plate, resistance of the adhesive with respect to the charge transfer by the patch and finally the detachment of the patch. The force-displacement curve shown in figures 13 and 14 shows a nearly linear behavior until the maximum load is reached for each repair case depending on the adhesive used. Then, the load capacity of the repaired structure increases from about 15% to 45% of the peak load. The charge continues to increase until it reaches a second point, about 10% to 20% of that of the last charge. The system maintains this level until a second fall, followed by the last point which represents the fracture of the structure.

However, the damage to the structure repaired by adhesive 7752 (Figure 15) does not follow the same path as the other two structures successively repaired by AV138 and Araldite 420. This difference comes from the 7752 adhesive which is by its very nature is more ductile which and subsequently confers a significant capacity of reinforcement to the structure.

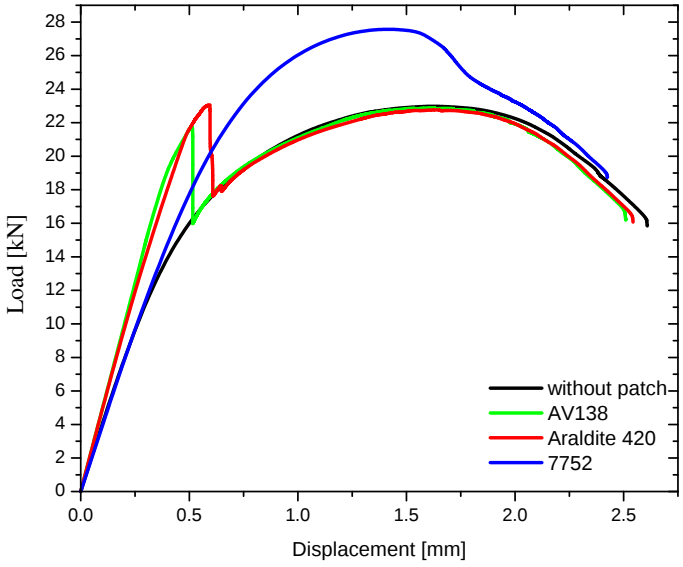

Figure 12. Failure load-displacement curves for different adhesives used.

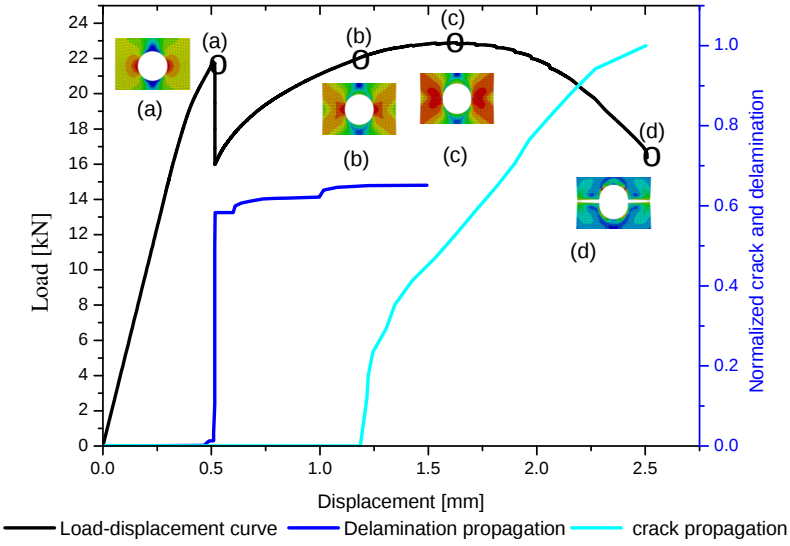

Figure 13. Force-displacement curve, the normalized crack length and debonding area for the case with circular notch of $r = a = b = 10\,\text{mm}$ with cohesive Araldite 420; (a) start of delaminating patch, (b) start of crack propagation in plate, (c) failure load, (d) total damage of aluminum plate.

The result of the numerical modeling in terms of force-displacement curve shows a good agreement of the detachment of the patch and the propagation of the crack according to the nature of the adhesive.

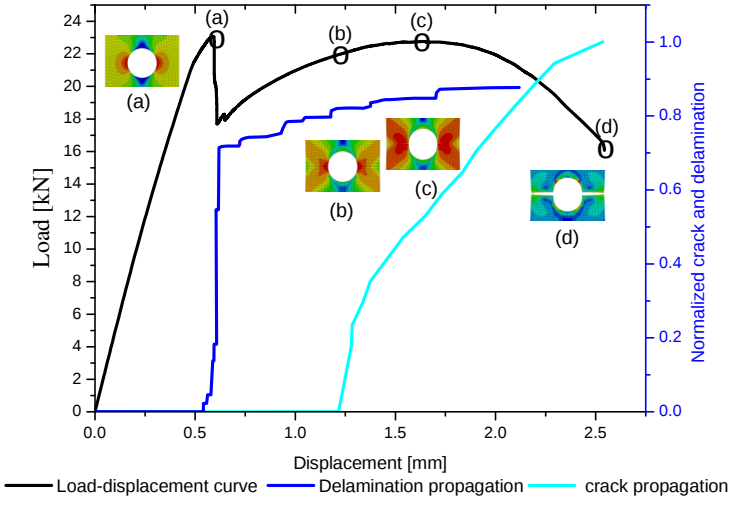

Figure 14. Force-displacement curve, the normalized crack length and debonding area for the case with circular notch of $r = a = b = 10\,\text{mm}$ with cohesive AV138; (a) start of delaminating patch, (b) start of crack propagation in Aluminium plate, (c) total damage of aluminum plate, (d) failure load.

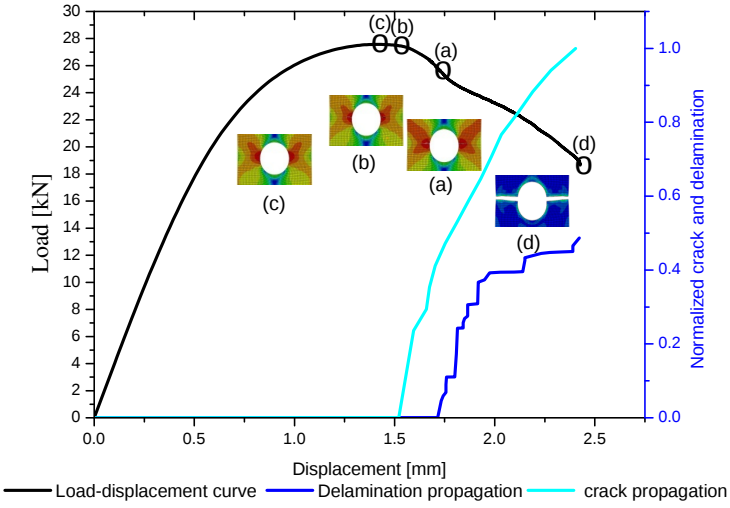

Figure 15. Force-displacement curve, the normalized crack length and debonding area for the case with circular notch of $r = a = b = 10$ mm with cohesive 7752; (a) start of delaminating patch, (b) start of crack propagation in aluminum plate, (c) failure load, (d) total damage of aluminum plate.

The first instantaneous decrease in load capacity is followed by the detachment of the composite patch (position (a)) and then the crack propagates once the load is reached at position (b) (figures 13 and 14). This behavior is observed for the case of structure repaired by bonding the patch by adhesives AV138 and Araldite 420.

The von Mises stress level presented in figures 16, 17 and 18 shows some events developed during the loading for different imposed displacements. For adhesive 7752 which exhibits more resistance to the

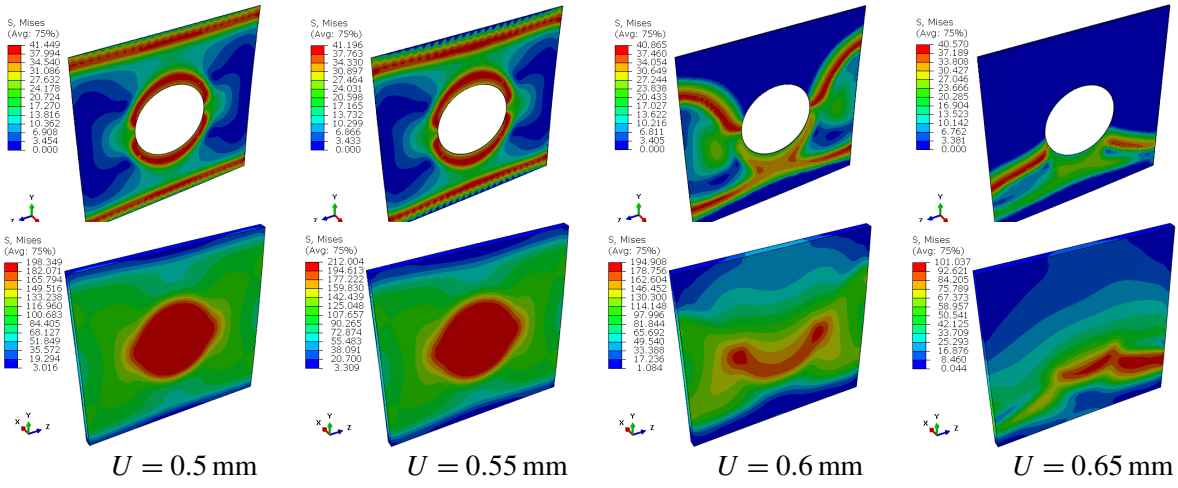

Figure 16. Von Mises stresses in the adhesive Araldite 420 and the composite patch for different imposed displacements U.

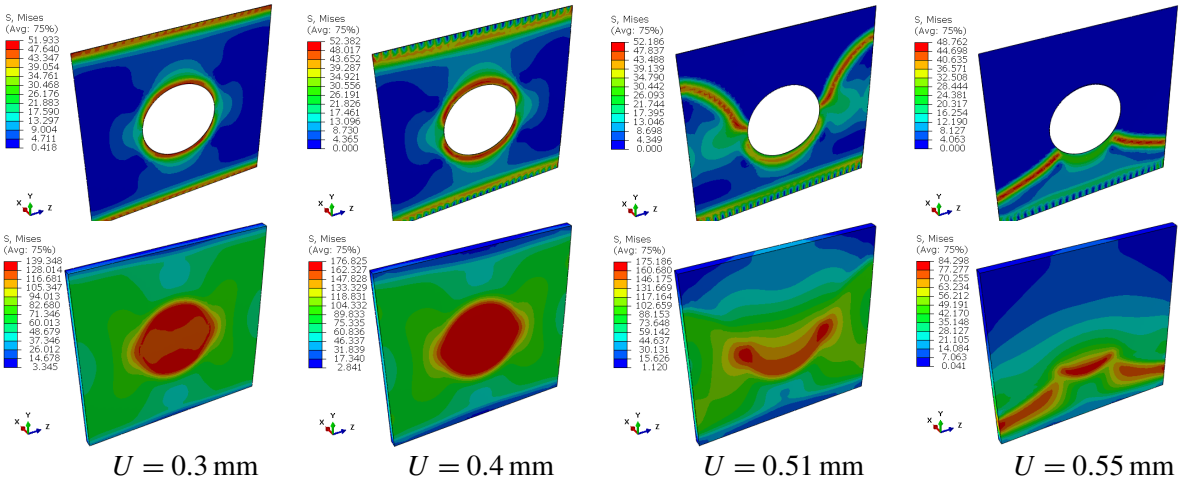

Figure 17. Maximal von Mises stresses in the adhesive AV138 and the composite patch for different imposed displacements U.

other two adhesives, crack propagation and patch detachment occur late. The crack propagates around an imposed displacement of 1.5 mm is followed by the detachment of the patch around an imposed displacement of 1.75 mm (Figure 18), which results in the good resistance of the adhesive to transfer the load from the damaged area to the composite patch and thus a good resistance of the repaired structure. However, in the case of repair of the structure by the two other adhesives, the propagation of the crack and the detachment of the patch occur at low values of the displacement imposed which confers a bad resistance to the structure.

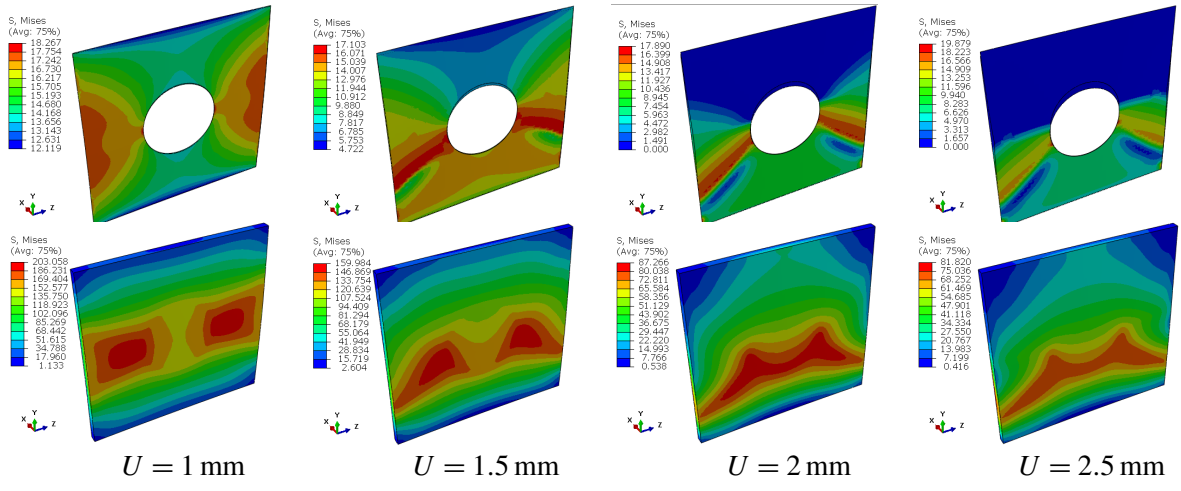

Figure 18. Maximal von Mises stresses in the adhesive 7752 and the composite patch for different imposed displacements U.

4. Conclusion

The present work demonstrated the effectiveness of a 3D modeling of the rupture behavior of a composite repaired structure by simultaneous analysis of crack propagation and patch detachment by two combined modeling techniques, cohesive zone model (CZM) and the XFEM technique. The competition between these two phenomena of damage (detachment of the patch and propagation of the crack) analyzed in a single numerical model advantageously makes it possible to evaluate these two parameters independently. The numerical results obtained in this study make it possible to deduce the following conclusions:

- The predictive capabilities of the modeling used on which we base ourselves allowed us to evaluate and compare different parameters conditioning damage to complex structures (reinforced by a composite patch).
- The structure accumulates two damages one after the other, thanks to the separation-traction law put in place.
- The strength of the patch depends on the size and shape of the notch.
- Stacking is one of the parameters that affects the reinforcement capacity: the least rigid in the sense of the load absorbs more load by its deformation.
- The strength of the adhesive used plays a decisive role in the reinforcement or repair capacity.
- The competition between the propagation of the crack in the plate and the detachment of the patch and conditioned by the strength of the adhesive and the dimensions of the reinforced structure, it could well be that it is a stronger adhesive.
- In all cases, plate damage analysis occurs at the notch around which the structure is weakened, but in most cases the detachment will remain at the edge of the patch.

In light of the above arguments, this work has provided appropriate modeling for more problems, based on predictions of cracks and detachments in repaired structures, and may also be of interest for further investigation.

References

[Ait Kaci et al. 2017] D. Ait Kaci, K. Madani, M. Mokhtari, X. Feaugas, and S. Touzain, "Impact of composite patch on the J-integral in adhesive layer for repaired aluminum plate", *Adv. Aircr. Spacecr. Sci.* **4**:6 (2017), 679–699.

[Belytschko and Black 1999] T. Belytschko and T. Black, "Elastic crack growth in finite elements with minimal remeshing", *Int. J. Numer. Methods Eng.* **45**:5 (1999), 601–620.

[Benzaama et al. 2018] A. Benzaama, M. Mokhtari, H. Benzaama, S. Gouasmi, and T. Tamine, "Using XFEM technique to predict the damage of unidirectional CFRP composite notched under tensile load", *Adv. Aircr. Spacecr. Sci.* **5**:1 (2018), 129–139.

[Campilho et al. 2013] R. D. S. G. Campilho, M. D. Banea, J. A. B. P. Neto, and L. F. M. da Silvac, "Modelling adhesive joints with cohesive zone models: effect of the cohesive law shape of the adhesive layer", *Int. J. Adhes. Adhes.* **44** (2013), 48–56.

[Elhannani et al. 2016] M. Elhannani, K. Madani, M. Mokhtari, S. Touzain, X. Feaugas, and S. Cohendoz, "A new analytical approach for optimization design of adhesively bonded single-lap joint", *Struct. Eng. Mech.* **59**:2 (2016), 313–326.

[Ezzine et al. 2018] M. C. Ezzine, A. Amiri, M. Tarfaoui, and K. Madani, "Damage of bonded, riveted and hybrid (bonded/riveted) joints: experimental and numerical study using CZM and XFEM methods", *Adv. Aircr. Spacecr. Sci.* **5**:5 (2018), 595–613.

[Ibrahim et al. 2016] N. C. Ibrahim, M. F. Bouanani, B. A. B. Bouiadjra, and B. Serier, "Analysis of the adhesive damage between composite and metallic adherends: application to the repair of aircraft structures", *Adv. Mater. Res.* **5**:1 (2016), 11–20.

[Jiao et al. 2017] P. Jiao, S. Soleimani, Q. Xu, L. Cai, and Y. Wang, "Effect of curing conditions on mode-II debonding between FRP and concrete: a prediction model", *Comput. Concrete* **20**:6 (2017), 635–643.

[Madani et al. 2010] K. Madani, S. Touzain, X. Feaugas, S. Cohendouz, and M. Ratwani, "Experimental and numerical study of repair techniques for panels with geometrical discontinuities", *Comput. Mater. Sci.* **48**:1 (2010), 83–93.

[Moës et al. 1999] N. Moës, J. Dolbow, and T. Belytschko, "A finite element method for crack growth without remeshing", *Int. J. Numer. Methods Eng.* **46**:1 (1999), 131–150.

[Mohamed and Bouiadjra 2016] B. Mohamed and B. B. Bouiadjra, "Analysis of the adhesive damage for different patch shapes in bonded composite repair of corroded aluminum plate", *Struct. Eng. Mech.* **59**:1 (2016), 123–132.

[Mokhtari et al. 2017] M. Mokhtari, K. Madani, H. Benzaama, and S. Malarino, "Effects of the composite stacking sequence on the failure load of the single lap bonded joint", *J. Theor. Appl. Mech.* (*Warsaw*) **55**:4 (2017), 1257–1268.

[Qian and Jing 2012] Z.-D. Qian and H. Jing, "Fracture properties of epoxy asphalt mixture based on extended finite element method", *J. Cent. South Univ.* **19** (2012), 3335–3341.

[Song et al. 2016] S.-I. Song, K.-S. Kim, and H.-G. Kim, "Estimation of a mixed-mode cohesive law for an interface crack between dissimilar materials", *Multiscale Multiphys. Mech.* **1**:1 (2016), 35–51.

Received 1 Jun 2019. Revised 8 Jan 2020. Accepted 29 Jan 2020.

MOHAMMED AMINE BELLALI: b.med.amine@live.fr
Mechanical Engineering Department, Djillali Liabes University of Sidi Bel Abbes, 22000 Sidi Bel Abbes, Algeria

MOHAMED MOKHTARI: mokhtarimohamed44@yahoo.fr
Mechanical Engineering Department, École Nationale Polytechnique Maurice Audin, RTFM, 31000 Oran, Algeria

HABIB BENZAAMA: habenza@yahoo.fr
Mechanical Engineering Department, École Nationale Polytechnique Maurice Audin, LABAB, 31000 Oran, Algeria

FEKIRINI HAMIDA: hamida.fekirini@univ-sba.dz
Department of Mechanical Engineering, Djillali Liabes University of Sidi Bel Abbes, 22000 Sidi Bel Abbes, Algeria

BOUALEM SERIER: *Department of Mechanical Engineering, Djillali Liabes University of Sidi Bel Abbes, LMPM, 22000 Sidi Bel Abbes, Algeria*

KOUIDER MADANI: koumad10@yahoo.fr
Department of Mechanical Engineering, Djillali Liabes University of Sidi Bel Abbes, LMPM, 22000 Sidi Bel Abbes, Algeria

JOURNAL OF MECHANICS OF MATERIALS AND STRUCTURES

msp.org/jomms

Founded by Charles R. Steele and Marie-Louise Steele

Cover photo: Mando Gomez, www.mandolux.com

See msp.org/jomms for submission guidelines.

JoMMS (ISSN 1559-3959) at Mathematical Sciences Publishers, 798 Evans Hall #6840, c/o University of California, Berkeley, CA 94720-3840, is published in 10 issues a year. The subscription price for 2020 is US $660/year for the electronic version, and $830/year (+$60, if shipping outside the US) for print and electronic. Subscriptions, requests for back issues, and changes of address should be sent to MSP.

JoMMS peer-review and production is managed by EditFLOW® from Mathematical Sciences Publishers.

PUBLISHED BY

mathematical sciences publishers

nonprofit scientific publishing

http://msp.org/

Journal of Mechanics of Materials and Structures

Volume 15, No. 2 March 2020

1559-3959(2020)15:2;1-K